

Performance of energy harvesters with parameter mismatch

Tomasz Burzyński¹, Piotr Brzeski², and Przemysław Perlikowski³

^{1,2,3}Division of Dynamics, Lodz University of Technology

Abstract

This study explores the impact of parameter mismatch on the stability of cross-well motion in energy harvesters, using a basin stability metric. Energy harvesters, essential for converting ambient energy into electricity, increasingly incorporate multi-well systems to enhance efficiency. However, these systems are sensitive to initial conditions and parameter variations, which can affect their ability to sustain optimal cross-well motion—a state associated with maximum power output. Our analysis compared four harvester types under varying levels of parameter mismatch, assessing resilience of the devices to parameter variations. By identifying safe operating ranges within the excitation parameter space, this study provides practical guidance for designing robust, stable harvesters capable of maintaining cross-well motion despite parameter uncertainties. These insights contribute to advancing the reliability of energy harvesting devices in real-world applications where parameter mismatches are inevitable.

Keywords: Energy harvesting, multistability, sample-based approach, basin stability

1 Introduction

Energy harvesting technology has witnessed rapid growth in popularity over the past decades. SCOPUS data indicates an almost exponential rise in interest since 2003. Specifically, the keyword "Energy harvesting" appeared in approximately 250 papers in 2003, around 1300 papers in 2009, about 5000 papers in 2015, and close to 9000 papers in 2023. The number of articles published up to July 2024 (around 9000) suggests that even more papers may be published by the end of the year.

Energy harvesters are employed in various scientific fields to replace conventional energy sources and generate electricity from ambient vibrations. The primary objective of energy harvesting technology is to maximize power generation under given excitation amplitudes and frequencies. The frequency spectra considered vary based on the intended use. For instance, energy harvesters for wearable devices aim to operate in the low-frequency range (1–10Hz), [1, 2], similar to those used for capturing energy from ocean waves [3]. Conversely, energy scavenging from vehicles, such as trains, occurs in the frequency spectrum of 20–65Hz [4, 5]. When the excitation frequency matches the device's natural frequency, increased power output is observed which is manifested by spikes on the frequency response curves (FRC). To achieve a more complex FRC, with more spikes and higher power output, systems with multiple potential wells are employed. Multi-well systems have become a standard in energy harvesting technology, and recently harvesters are have become increasingly sophisticated and non-linear to further extend the operation range.

Recent studies provide illustrative examples. Li et al. in [6] introduced a classical bistable mechanical electromagnetic energy harvester augmented with a non-linear boundary, incorporating strong Duffing-type non-linearities to enhance energy harvesting. Zhang et al. [7] tried to increase device performance by introducing a discontinuity in the form of impacts to the model, the same applies to the work of Wang et al. [8]. Additional mass and springs are added to the classical piezoelectric energy harvester by Chen et al [9]. A strong negative stiffness is introduced to the classical harvester model by Chen and Zhao [10] to create so-called quasi-zero stiffness oscillator and facilitate energy scavenging. These examples demonstrate that various non-linearities and discontinuities are introduced to enhance device performance, albeit at the cost of increased multistability, which has become an inherent aspect of energy harvesting from electromechanical devices.

Considering a bistable system with two potential wells, commonly used in energy harvesting, such systems possess three equilibrium positions: one unstable and two stable. These systems can exhibit qualitatively different behaviors, including oscillations around one equilibrium position, transitions between two equilibrium positions, oscillations with significant amplitude encompassing both extreme equilibrium positions, and chaotic motion. Cross-well motion between two extreme equilibrium positions is most favorable for maximizing power

output. This fact was observed by Sosna et al. [5] in piezoelectric energy harvester. The same was reported by Li et al. [11]. The electromagnetic device was analyzed with the same conclusions by Chen et al. [12], here authors also emphasize the drop in power output during chaotic motion. Tang et al. [13] in his work introduced variable damping control to a piezoelectric harvester to activate high-energy response that corresponds to cross-well motion. Yan et al. [14] studied a quad-stable energy harvester with four stable equilibrium positions, finding optimal operation during quad-well motion spanning extreme equilibrium positions.

Taking into consideration the examples given, the assessment of device's effectiveness can be reduced to the ability to reach and maintain cross-well motion. Because considered systems are multistable, hence initial conditions sensitive, we focus on the probability of reaching cross-well motion. When it comes to probabilistic analysis of multistable systems, basin stability metrics, and sample-based approach are good candidates for the measures used to assess the systems [15, 16]. The analysis may be further extended by adding parameters mismatch [17], since harvesters include complex interactions between mechanical and electrical subsystems that are challenging to model.

The novelty in this study is to use basin stability type metric with parameter mismatch to assess the effectiveness of the energy harvesters based on the system response dynamics rather than on the power output. The goal of the study is to answer the following questions: What are the excitation parameters when the cross-well motion has the greatest basin stability regardless of the parameters mismatch? How different types of systems are prone to parameter mismatch? What degree of parameter mismatch is significant?

2 Materials and methods

In this paper, we focus on calculating the probability of reaching stable cross-well motion in four different energy harvesters. For this purpose, we employ the basin stability method with parameter mismatch, first introduced by Brzeski et al. in [17] to detect and classify coexisting solutions in non-linear systems. It is an extension of the original basin stability method introduced by Menck et al. [18]. Basin stability with parameter mismatch assumes that the exact values of chosen parameters are unknown due to finite precision, indirect measurement methods or their variability during motion (e.g., dependence on displacement, velocity or ect.). This results in an additional variance between the real-world system and the numerical model, affecting the overall accuracy of the mathematical approximation.

We examine how this variance influences the model by determining whether the solution obtained for fixed parameter values remains the sole possible attractor or at least maintains a major basin of attraction when the chosen parameters fluctuate. This approach can be considered a type of stability analysis, where we investigate how the system dynamics may

change due to system degradation or significant misjudgment of parameter values.

In our study, we assume that two parameters (excitation amplitude and frequency) define a 2D space where we investigate the system dynamics. These parameters are drawn from pre-defined sets using the Monte Carlo approach. Additionally, we vary other parameters that are difficult to identify or prone to change as the system wears. For each parameter, we assume a reference value, believed to be the real one, and observe how the system dynamics change as these parameters vary by $\pm 2.5\%$, $\pm 5\%$, and $\pm 10\%$. For every system, we specify which parameters are mismatched, but for most systems these are: viscous damping, electromechanical coupling coefficients, and parameters defining the system's potential energy. We choose these parameters because mechanical damping in all considered systems is expressed by viscous damping. Energy dissipation is a complex phenomenon, often involving multiple sophisticated processes simultaneously alongside viscous damping. Therefore, we assume that describing the entire phenomenon with a viscous model is challenging, making damping coefficients good candidates for parameter mismatch. The same applies to electromechanical coupling coefficients, which are linearized and proportional to velocity/current, while the actual interactions between mechanical and electrical subsystems are far more complex (see, for example, [19], where the authors optimize the parameters of a mathematical model of a coil, or [20], where the electromagnetic coupling coefficient is a function of the magnet's position relative to the coil). Additionally, system stiffness may degrade as the system wears, so we also consider stiffness parameters during mismatch.

In this paper, we investigate four energy harvesters, two of electromagnetic and two of piezoelectric type. The first model is derived from the beginning, while the others are introduced and derived in referenced papers [21, 6, 8]. Detailed information about these models can be found in those sources. Figure 1 presents schematic diagrams of all systems, providing a comprehensive comparison and showing their variety. This figure should not be treated as a detailed representation of the physical models used for deriving the mathematical models, as those details are available in the original papers (except for the first system). Relevant descriptions of the systems and their mathematical models are presented in the following subsections.

2.1 Classical bistable energy harvester (S1)

The first system (S1) is a bistable mechanical oscillator. The physical model of the device is presented in 1a. Bistability results from the geometry of the system that consists only of elements with linear response. Mass attached to two springs oscillates and moves the magnet inside a coil. The stiffness of the system is controlled by varying the distance between the spring mounting point and the translational axis of the oscillator - parameter h . By proper parameter tuning, we can obtain strong non-linear stiffness. System configuration presented

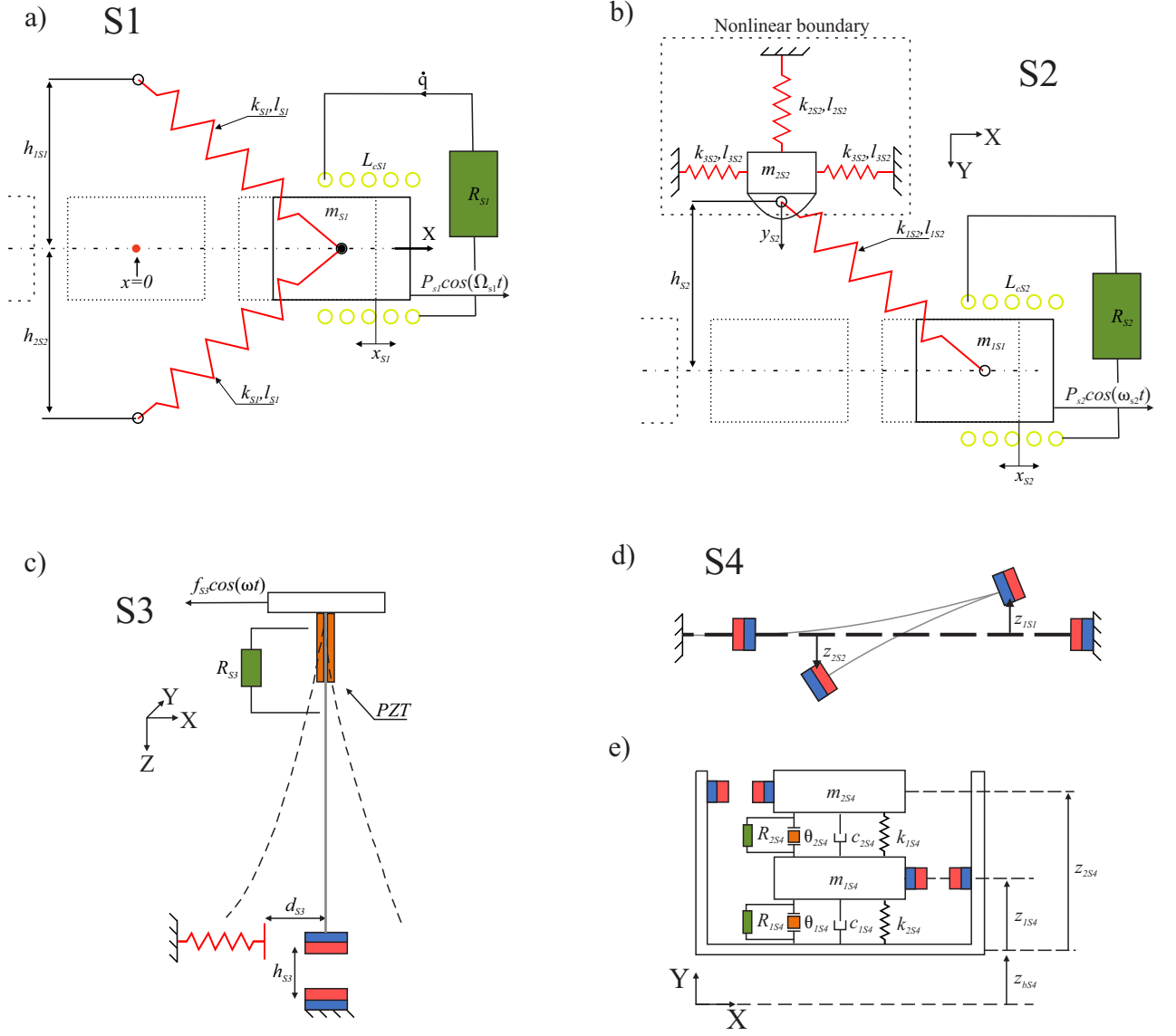


Figure 1: Schematic diagrams of four investigated systems. a) Classical electromagnetic bistable energy harvester (S1). b) Electromagnetic bistable energy harvester with non-linear boundary (S2), introduced by [6]. c) Asymmetric piezoelectric energy harvester (S3), introduced by [8]. d,e) Two degrees of freedom piezoelectric energy harvester (S4), introduced by [21].

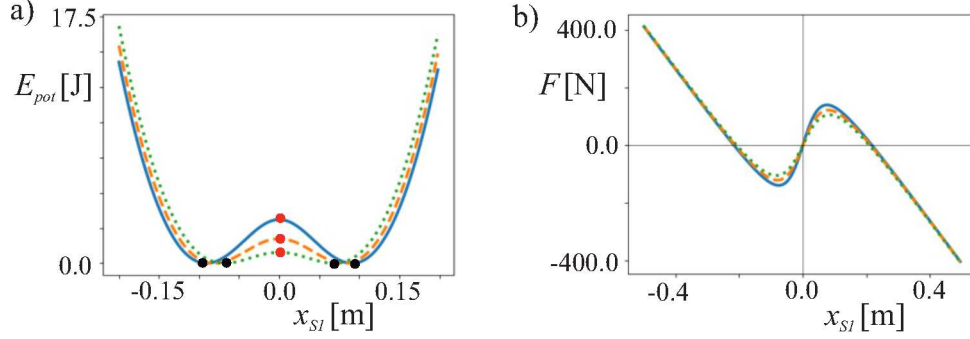


Figure 2: a) Elastic potential energy of S1 for different values of h parameter. Red dots represents unstable equilibrium positions, black dots stable equilibrium positions. Blue solid line is for $h_{1S1} = h_{2S1} = 0.6l_0$, orange dashed for $h_{1S1} = h_{2S1} = 0.7l_0$, green dotted for $h_{1S1} = h_{2S1} = 0.8l_0$ b) Restoring force (in X direction) generated by spring along X axis.

in 1(a) demonstrates three equilibrium positions marked with dots on the X axis. A red dot means unstable equilibrium, black dot stable equilibrium (only one stable equilibrium is presented but the other one, symmetric, exists on the other side). Figure 2 shows the elastic potential energy of the device and the stiffness of the system along the X axis for different values of h parameter. We can observe a typical double-well potential landscape and the phenomena of negative stiffness that is typical for such a system. In this system configuration, we may observe different behaviors like oscillations around one of the equilibrium positions, jumping between two different equilibrium positions, and oscillations with significant amplitude spanning both extreme equilibrium positions.

The considered system consists of electrical and mechanical subsystems. The mathematical model possesses two generalized coordinates - mechanical variable x which is the translational displacement of the mass attached to the springs and electrical variable q which is an electric charge. The magnet moving inside the coil is a coupling terminal that demonstrates the interaction between the mechanical and electrical subsystems. The coupling is originated from the magnetic energy of the system. For the electrical subsystem, we define magnetic coenergy, derived according to [22], as:

$$W = \frac{L_{cS1}\dot{q}^2}{2} + \alpha_{S1}\dot{q}x, \quad (1)$$

where, L_c is inductance of the coil, α is electromagnetic force constant. Translational kinetic energy and elastic potential energy for the system are:

$$T = \frac{m_{S1}\dot{x}^2}{2},$$

$$V = k_{S1} \left(l_{S1} - \sqrt{x^2 + h_{1S1}^2} \right)^2 + k_{S1} \left(l_{S1} - \sqrt{x^2 + h_{2S2}^2} \right)^2.$$

Generalized forces for the mechanical and electrical subsystems are presented below:

$$Q_m = A \cos(\omega t) - d\dot{x},$$

$$Q_e = -R_{S1}\dot{q},$$

where, A is an amplitude of the external mechanical excitation, d is the coefficient of energy dissipation due to internal resistances, R_{S1} is the sum of electrical resistance in the system. Equations of motion are derived using Lagrange's equations of second kind:

$$\frac{d}{dt} \left(\frac{\partial \mathcal{L}}{\partial \dot{x}} \right) - \frac{\partial \mathcal{L}}{\partial x} = Q_m, \quad (2)$$

$$\frac{d}{dt} \left(\frac{\partial \mathcal{L}}{\partial \dot{q}} \right) - \frac{\partial \mathcal{L}}{\partial q} = Q_e, \quad (3)$$

where Lagrangian is defined as $\mathcal{L} = T - V + W$. Using following substitutions for the general coordinates: $\tau = \omega_{nS1}t$, $x = \bar{x}l_0$, $\dot{q} = \dot{\bar{q}}i_0$, where, $\omega_{nS1} = \sqrt{\frac{k_{S1}}{m_{S1}}}$, l_{S1} is the free length of the spring, and i_0 is some reference current, equations are made dimensionless (means derivative with respect to τ):

$$\begin{aligned} \ddot{\bar{x}} + \bar{x} \left(1 - \frac{1}{\sqrt{\bar{x}^2 + \gamma_1^2}} \right) + \bar{x} \left(1 - \frac{1}{\sqrt{\bar{x}^2 + \gamma_2^2}} \right) - \theta \dot{\bar{q}} &= P_{S1} \cos(\Omega_{S1}\tau) - \varphi \dot{\bar{x}}, \\ \ddot{\bar{q}} + \varepsilon \dot{\bar{x}} + \lambda \dot{\bar{q}} &= 0, \end{aligned}$$

including dimensionless parameters:

$$\begin{aligned} \Omega &= \frac{\omega}{\omega_{nS1}}, \quad \gamma_1 = \frac{h_1}{l_0}, \quad \gamma_2 = \frac{h_2}{l_0}, \quad \theta = \frac{\alpha_{S1}i_0}{l_0k_{S1}}, \quad \varphi_{S1} = \frac{D}{\sqrt{k_{S1}m_{S1}}}, \quad \varepsilon = \frac{\alpha_{S1}l_0}{L_{cS1}i_0}, \\ \lambda_{S1} &= \frac{R_{S1}}{L_{cS1}\sqrt{\frac{k_{S1}}{m_{S1}}}}, \quad P = \frac{A}{l_0k_{S1}} \end{aligned}$$

where:

$$m_{S1} = 0.2 \text{ [kg]}, \quad l_0 = 0.114 \text{ [m]}, \quad h_1 = h_2 = 0.95l_0 \text{ [m]}, \quad L_{cS1} = 1.463 \text{ [H]},$$

$$\alpha_{S1} = 30 \left[\frac{N}{A} \right], \quad c_{S1} = 0.35 \left[\frac{Ns}{m} \right], \quad k_{S1} = 1500 \left[\frac{N}{m} \right], \quad R_{S1} = 2200 \text{ [\Omega]}.$$

Values of electrical subsystem parameters α_{S1} , L_{cS1} , R_{S1} were taken from [23] for a similar real-world electromagnetic system. Spring parameters k_{S1} , l_0 are obtained by measuring existing products whose size and stiffness correspond to the system dimensions. The chosen value of m_{S1} is not overloading spring elements and still corresponds in size to the system presented in [23]. Mechanical damping component c_{S1} is set to 2.5% of critical damping of the system since extremely low friction joints need to be used to assure the efficiency of such a device.

2.2 Bistable energy harvester with non-linear elastic boundary (S2)

The second system (S2) is the expansion of the first one. System S2 also consists of a magnet inside a coil supported by the hinged spring in such a way that strong geometric non-linearity is created. What distinguishes the two systems is the non-linear elastic boundary. In S2 the boundary is introduced by a set of additional springs (k_{2S2} , k_{3S2}) that support the hinge. In S1 the hinged spring was assumed to have infinite stiffness support, in S2 the support is elastic. The system was introduced for the first time by Li et al. in [6], and detailed model descriptions can be found there. Governing dimensionless equations of motion are as follows:

$$\ddot{X} + X \left(1 - \frac{1}{\sqrt{X^2 + \eta_1^2 (1 - Y)^2}} \right) + \varphi_{1S2} \dot{X} = P_{S2} \cos(\omega_{S2} t) - \rho I$$

$$\ddot{Y} + \frac{\lambda}{\mu_1} Y + 2 \frac{\lambda}{\mu_2} Y \left(1 - \frac{1}{\sqrt{1 + \eta_2^2 Y^2}} \right) - \lambda (1 - Y) \left(1 - \frac{1}{\sqrt{X^2 + \eta_1^2 (1 - Y)^2}} \right) + \varphi_{2S2} \dot{Y} = 0$$

$$\dot{I} + \theta_{S2} I = \varepsilon \dot{X}$$

where, φ_{iS2} are dimensionless damping coefficients of the the 1st and 2nd mechanical degree of freedom, $\eta_1 = \frac{h_{S2}}{l_1}$, $\eta_2 = \frac{h_{S2}}{l_3}$ (see the figure 1b), P is dimensionless excitation amplitude, λ is mass ratio, ρ and ε are electromechanical coupling coefficients for electrical and mechanical

part respectively, $\mu_1 = \frac{k_1}{k_2}$, $\mu_2 = \frac{k_1}{k_3}$ (see the figure 1b). Values of the parameters are the following:

$$\lambda = 4 \quad \eta_1 = 0.92 \quad \eta_2 = 1.75 \quad \varphi_{1S2} = 0.005 \quad \varphi_{2S2} = 0.02 \quad \mu_1 = \mu_2 = 1$$

$$\theta = 20 \quad \varepsilon_{S2} = 13.13 \quad \rho = 0.005$$

2.3 Asymmetric piezoelectric bistable energy harvester (S3)

The third system (S3) is based on the simple form of the piezoelectric energy harvester with two repulsive magnets and a beam with a piezoelectric transducer attached. Additionally, there is a unilateral spring that limits the motion of the beam and introduces to the system asymmetry and soft impacts. The model was introduced by Wang et al. in [8] and detailed description can be found there. The system is governed by the following dimensionless equations:

$$\ddot{y} + 2\xi_{1S3}\dot{y} - y + \beta_{S3}y + \delta_{S3}y^3 + g(y, \dot{y}) - \kappa_{S3}^2 V = f_{S3} \cos(\omega_{S3}t)$$

$$\dot{V} + \alpha_{S3}V + \dot{y} = 0$$

$$g(y, \dot{y}) = \begin{cases} 0, & y > -d_{S3} \\ 2\xi_{2S3}\dot{y} + K_{S3}(y + d_{S3}), & y \leq -d_{S3} \end{cases}$$

where, ξ_{1S3} and ξ_{2S3} are dimensionless damping ratios, β_{S3} and δ_{S3} are dimensionless coefficients characterizing non-linear restoring forces, κ_{S3} is dimensionless electromechanical coupling coefficient, d_{S3} is the dimensionless distance marked in the figure 1c, K_{S3} is dimensionless collision stiffness, ω_{S3} is dimensionless excitation frequency, and f_{S3} is dimensionless excitation amplitude. The values of parameters are as follows:

$$\xi_{1S3} = 0.08 \quad \xi_{2S3} = 0.05 \quad \beta_{S3} = 0.25 \quad \delta_{S3} = 0.5 \quad \kappa_{S3} = \sqrt{0.002} \quad \alpha_{S3} = 0.4 \quad K_{S3} = 100 \quad d_{S3} = 0.6$$

2.4 Compact non-linear piezoelectric energy harvester (S4)

Fourth system (S4) is a two-degree-of-freedom piezoelectric energy harvester that consists of two coupled beams and four magnets as indicated in the figure 1d and e. It is an expansion of the system S3 but without the asymmetric spring. This system is proposed by Costa et

al. in [21] and detailed information about the system can be found there. Dimensionless equations of motion of the system are given below:

$$\ddot{\bar{z}}_1 + 2\zeta_{1S4}\dot{\bar{z}}_1 - 2\zeta_{2S4}(\dot{\bar{z}}_2 - \dot{\bar{z}}_1) + (1 + \alpha_{1S4})\bar{z}_1 + \beta_{1S4}\bar{z}_1 - \rho_{S4}\Omega_s^2(\bar{z}_2 - \bar{z}_1) - \chi_{1S4}\bar{v}_1 + \chi_{2S4}\bar{v}_2 = -\ddot{\bar{z}}_b$$

$$\rho_{S4}\ddot{\bar{z}}_2 + 2\zeta_{2S4}(\dot{\bar{z}}_2 - \dot{\bar{z}}_1) + \alpha_{2S4}\bar{z}_2 + \beta_{2S4}\bar{z}_2 + \rho_{S4}\Omega_s(\bar{z}_2 - \bar{z}_1) - \chi_{2S4}\bar{v}_2 = -\ddot{\bar{z}}_b$$

$$\dot{\bar{v}}_1 + \varphi_{1S4}\bar{v}_1 + \kappa_{1S4}\dot{\bar{z}}_1 = 0$$

$$\dot{\bar{v}}_2 + \varphi_{2S4}\bar{v}_2 + \kappa_{2S4}(\dot{\bar{z}}_2 - \dot{\bar{z}}_1) = 0$$

where, $z_b = \gamma_{S4} \sin(\Omega_{S4}\tau)$ is the dimensionless excitation frequency, γ_{S4} is the dimensionless excitation amplitude, Ω_{S4} is the dimensionless excitation frequency, ρ_{S4} is ratio of masses, ζ_{iS4} are dimensionless mechanical damping coefficients of 1st and 2nd mechanical degree of freedom, Ω_s is ratio of linearized natural frequencies, α_{iS4} are dimensionless linear restitution coefficients, β_{iS4} are dimensionless non-linear restitution coefficients, χ_{iS4} are dimensionless piezoelectric coupling coefficients in the mechanical ODE, κ_{iS4} are dimensionless piezoelectric coupling coefficients in the electrical ODE, φ_{iS4} are dimensionless electrical resistance of the 1st and 2nd circuits. Values of parameters are as follows:

$$\zeta_{1S4} = \zeta_{2S4} = 0.025 \quad \alpha_{1S4} = -2 \quad \alpha_{2S4} = -1 \quad \beta_{1S4} = \beta_{2S4} = 1$$

$$\chi_{1S4} = \chi_{2S4} = 0.05 \quad \kappa_{1S4} = \kappa_{2S4} \quad \rho_{S4} = 1 \quad \Omega_s = 0.25 \quad \varphi_{1S4} = \varphi_{2S4} = 0.05$$

3 Results

This section presents basin stability with parameter mismatch metrics for different systems. Their dynamics is investigated in 2D parameter space that is divided into 1600 boxes. The color intensity of each box determines the probability of reaching cross-well motion in that part of the parameter space. The probability varies from 0 to 1, where 1 means that 100% of all samples demonstrate cross-well motion, otherwise there are other attractors. Each system is simulated four times (for different amounts of parameter mismatch) and each simulation includes 200000 samples. The number of samples was selected in such a way that each box contained at least 100 samples. Dimensionless excitation frequency and amplitude are presented on the horizontal and vertical axis respectively. Figure captions tell which other parameters were mismatched and what was the range of initial conditions considered.

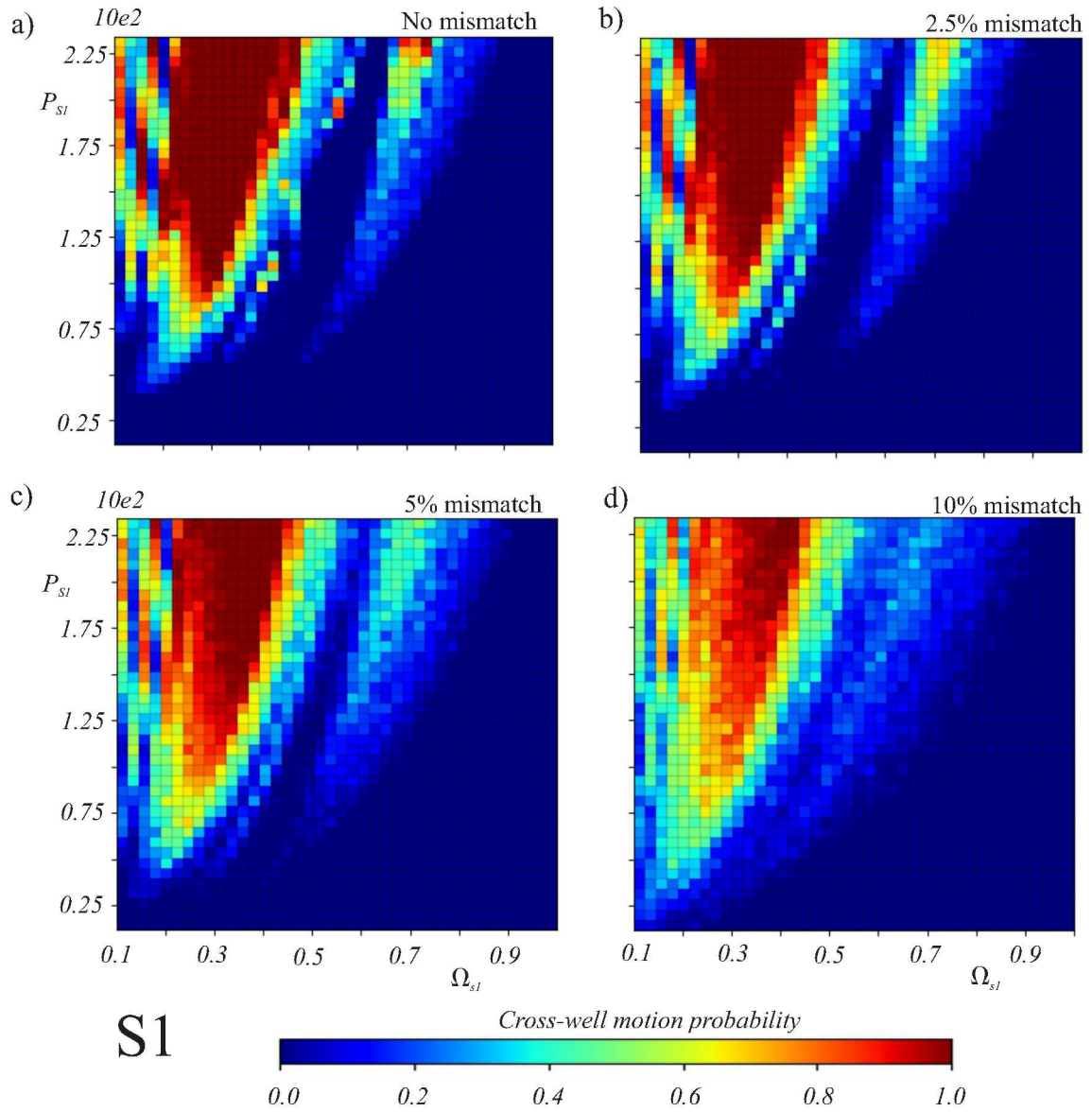


Figure 3: Probability of reaching stable cross-well motion for S1. Parameters that are mismatched: γ_{2S1} , θ_{S1} , ε_{S1} , φ_{S1} represent respectively: potential well shape, electromechanical coupling, and mechanical damping. Range of initial conditions: $\bar{x}_{S1}, \bar{\dot{x}}_{S1} \in (-1, 1)$ Degree of parameter mismatch: a) No mismatch b) $\pm 2.5\%$ c) $\pm 5\%$ d) $\pm 10\%$.

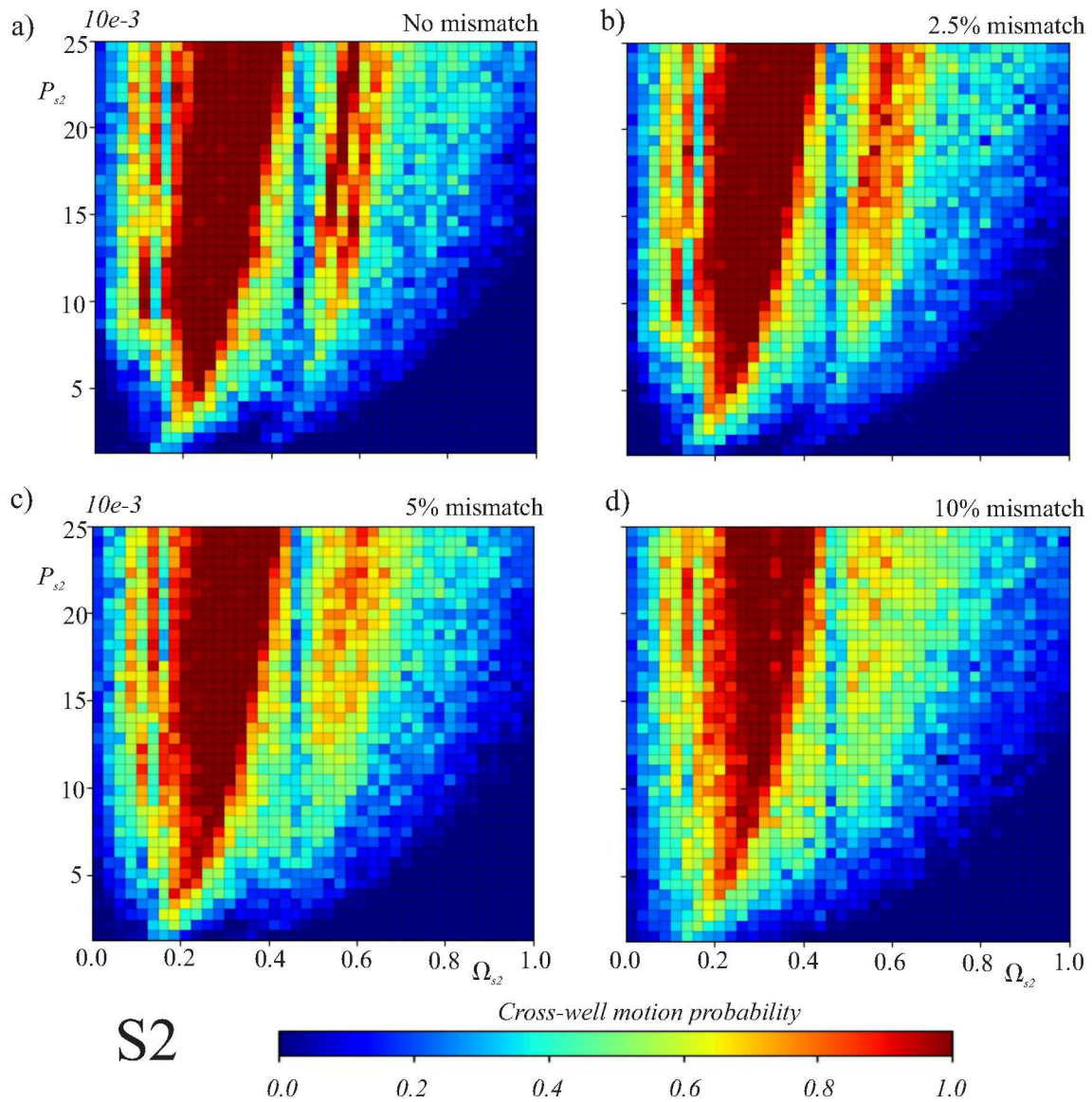


Figure 4: Probability of reaching stable cross-well motion for S2. Parameters that are mismatched: η_{1S2} , η_{2S2} , ρ_{S2} , ε_{S2} , φ_{1S2} , φ_{1S2} represent respectively: potential well shape, electromechanical coupling, and mechanical damping. Range of initial conditions: X , $\dot{X}\epsilon < -1, 1 >$ Degree of parameters mismatch: a) No mismatch b) $\pm 2.5\%$ c) $\pm 5\%$ d) $\pm 10\%$.

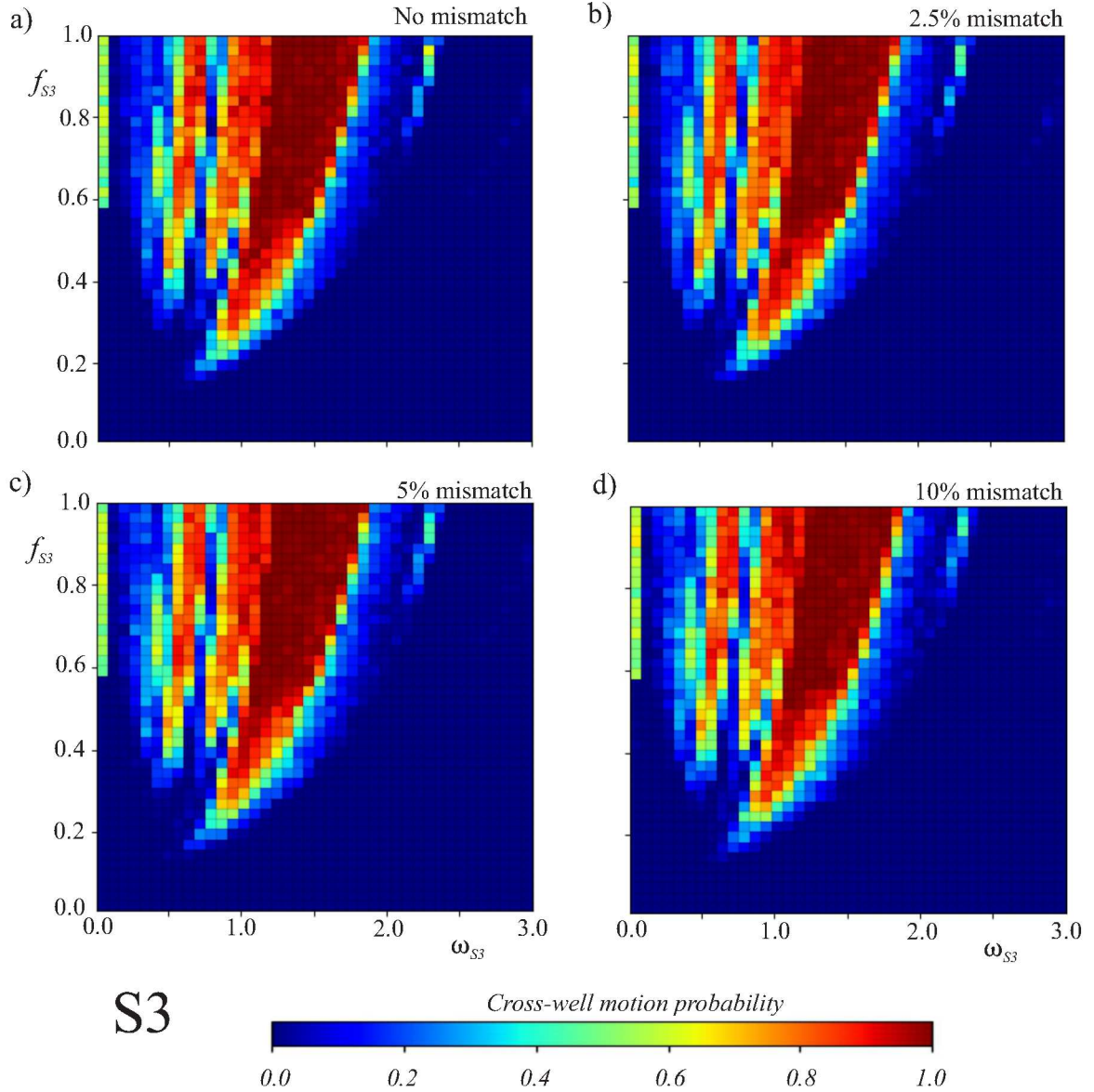


Figure 5: Probability of reaching stable cross-well motion for S3. Parameters that are mismatched: K_{S3} , κ_{S3} , ζ_{1S3} , ζ_{2S3} represent respectively: stiffness of the unilateral stop, electromechanical coupling, and mechanical damping. Range of initial conditions: $y\epsilon < -0.55, 2 >$, $\dot{y}\epsilon < -2, 2 >$ Degree of parameter mismatch: a) No mismatch b) $\pm 2.5\%$ c) $\pm 5\%$ d) $\pm 10\%$.

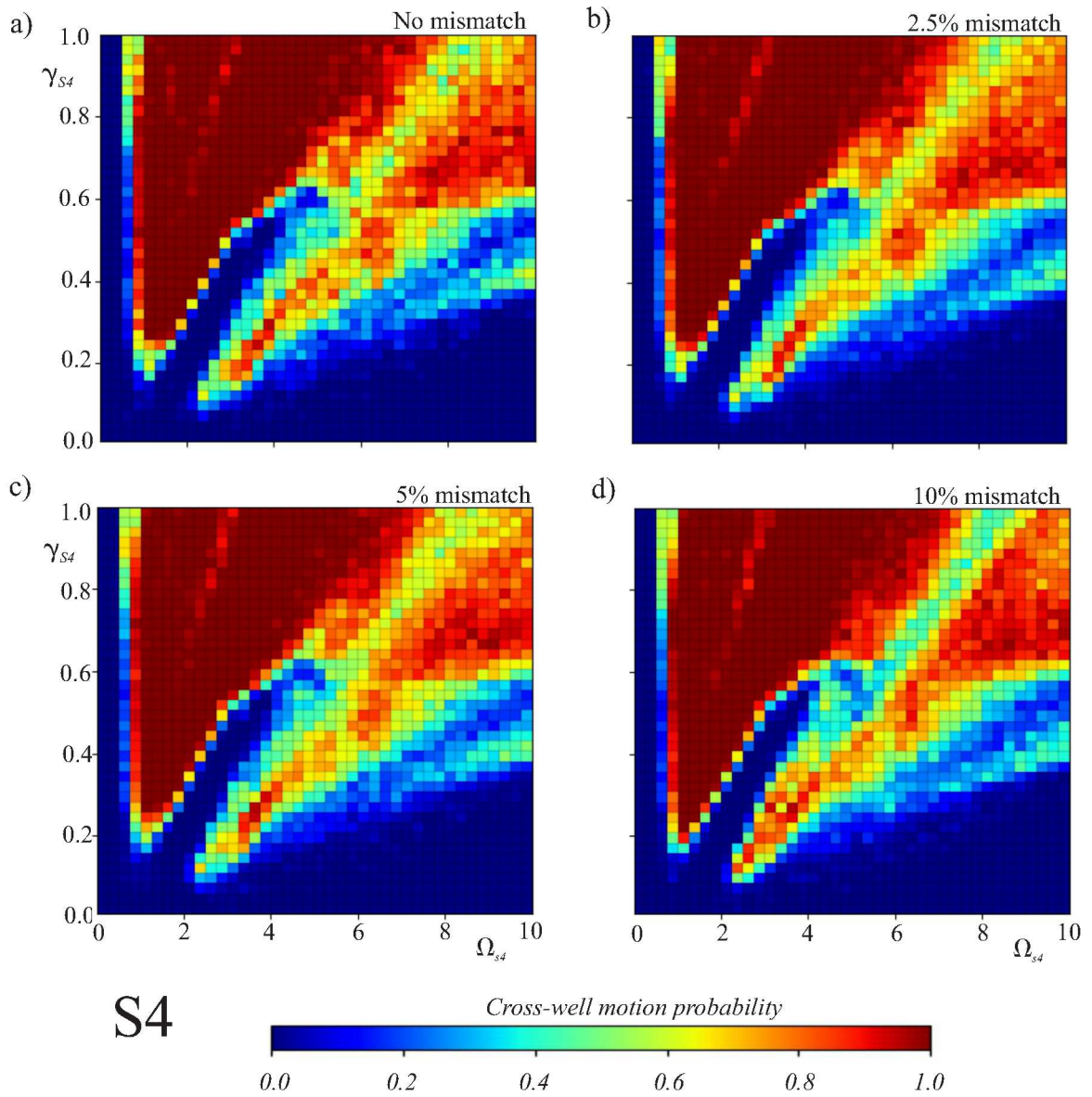


Figure 6: Probability of reaching stable cross-well motion for S4. Parameters that are mismatched: χ_{1S4} , χ_{2S4} , κ_{1S4} , κ_{2S4} , ζ_{1S4} , ζ_{2S4} represent respectively: electromechanical coupling coefficients, and mechanical damping. Range of initial conditions: $z_1 \in \langle -2, 2 \rangle$, $z_2 \in \langle -2, 2 \rangle$ Degree of parameter mismatch: a) No mismatch b) $\pm 2.5\%$ c) $\pm 5\%$ d) $\pm 10\%$.

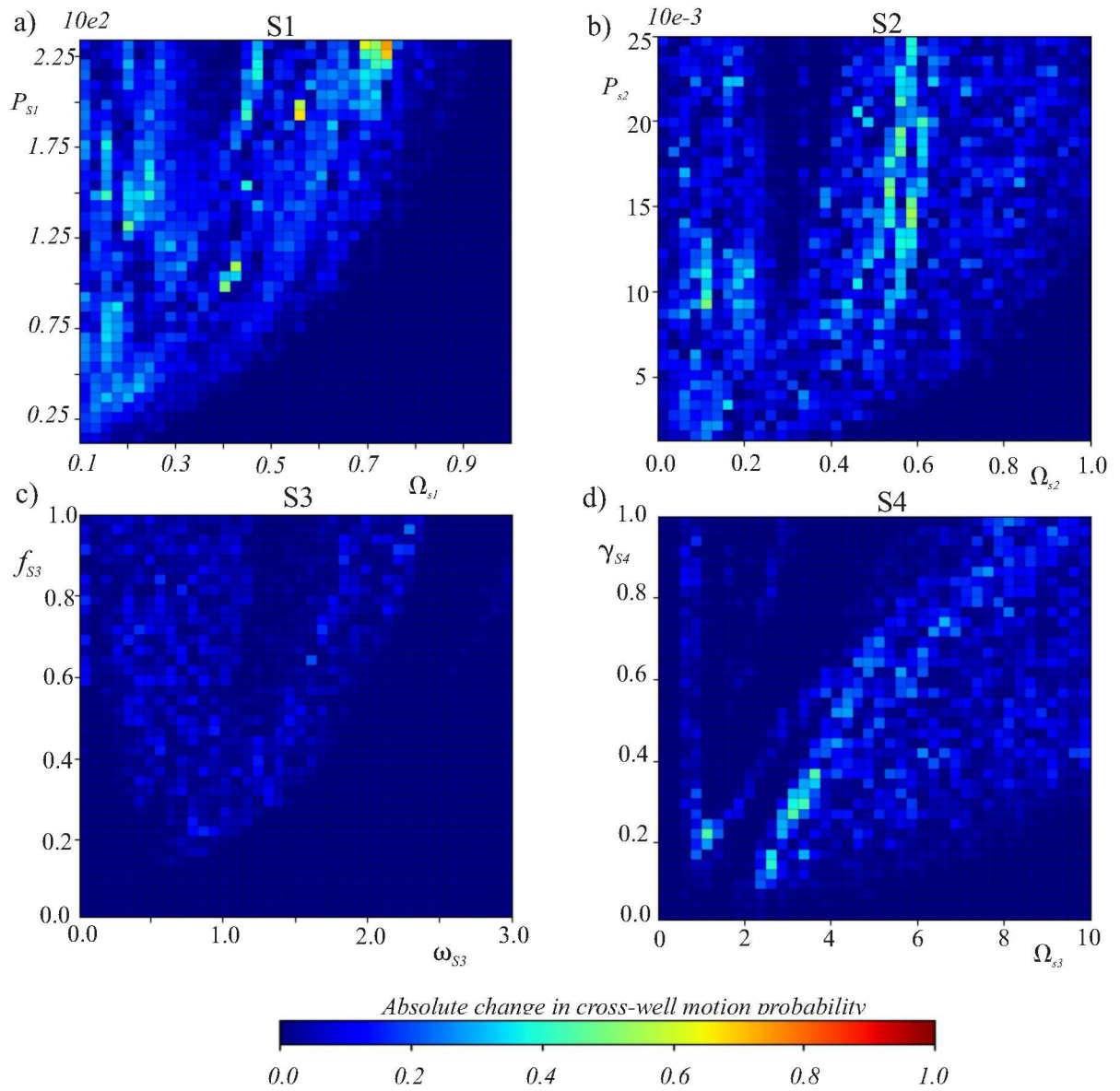


Figure 7: Change in cross-well motion probability while the parameters were mismatched $\pm 10\%$ a) S1 b) S2 c) S3 d) S4

Figure 3 shows results for S1. Panel (a) represents situation when all other parameters than excitation amplitude and frequency are fixed. We can observe a tongue-shaped region spanned from $\Omega_{S1}\epsilon < 0.2, 0.4 >$ and $P_{S1} > 1$ where the probability of reaching cross-well motion is 1. If we want to maximize the efficiency of the device it should operate in this parameter range. Panels (b), (c), and (d) show situations when we vary other parameters. These parameters are indicated in the figure caption. We observe the erosion of the probability of reaching stable cross-well motion. The greater the parameter mismatch, the greater the erosion. In panel (d) the regions with a 100% probability of cross-well motion are found only when $\Omega_{S1} = 0.4$ and $P_{S1} > 1.75$. Erosion progresses with increasing excitation amplitude and frequency values. In practice, it means that if the system was excited with $\Omega_{S1} = 0.3$ and $P_{S1} = 1.25$ assuming exact values of other parameters the model assures that the stable cross-well motion is the only existing attractor. However, if it turns up that the real values of chosen parameters (indicated in figure caption) are within 10% of assumed values the probability drops to $\approx 70\%$. Also the second tongue-shaped region with increased probability visible in figure 3(a) almost completely disappears in panel (d) of the same figure, indicating that it is susceptible to parameter change.

Figure 4 shows results for S2. Panel (a) represents a situation when all other parameters except excitation amplitude and frequency are fixed. The range of considered excitation frequency and amplitude corresponds to the values analyzed in the original paper [6]. The tongue-shaped region with the red color visible in panel (a) indicates which parameters provide the existence of solely the desired cross-well solution. S2 guarantees reaching this solution in a greater parameter range compared to S1. The model is more complex and stronger nonlinearity exists due to elastic boundary. However, similarly as in the previous case, we observe the erosion of probability of reaching cross-well motion as we increase parameter mismatch. Erosion progresses with increasing excitation amplitude and frequency values. The second smaller tongue does not disappear however the probability drops. When the parameter mismatch reaches $\pm 10\%$ the probability decreases to ≈ 0.6 while with fixed parameter values there were regions with probability equal to 1. The results for S2 show that in practice the second smaller tongue should not be considered an effective-operation region since it is sensitive to small parameter variations. Figure 4 shows what are the excitation parameter values when the main tongue-shaped regions ensure only one high-power attractor regardless of the parameter mismatch. This system also is characterized by a significant number of boxes with a probability between 0.4 and 0.6.

Figure 5 presents results for S3. The range of considered excitation frequency and amplitude correspond to the values analyzed in the original paper [8]. We can see on all panels that the region with the highest probability (boxes in shades of red) is not as uniform as in the two previous cases. For S3 in the shade red areas, probability varies between 0.9 and 1. For S1 and S2 there were uniform regions with probability equal to 1. Interestingly, at the

same time, there are only a few boxes where the probability is between 0.3 and 0.8 meaning that in practice we can assume only two possible outcomes (Major probability of reaching cross-well motion and major probability of reaching intra-well motion), except boundaries between these two regions where are the boxes with the shades of light blue and yellow. Even more interesting is the fact that parameter mismatch is not affecting significantly the probability of reaching cross-well motion. All four panels are qualitatively similar, implying that the system is resistant to parameter fluctuations.

Figure 6 shows results for S4. The range of considered excitation frequency and amplitude correspond to the values analyzed in the original paper [21]. We observe that the cross-well motion is obtained in a much greater range of frequencies than in all previous examples. There are two tongue-shaped regions, the first one on the left side of the plot ensures that the desired behavior of the system is almost solely possible (with a probability 0.9 or more). The second tongue-shaped region is more interwoven by different attractors and the probability of reaching cross-well motion varies between 0.3 and 1. Similarly as in the previous case (S3), this system is resistant to parameter mismatch, meaning that the system dynamics is not affected even if parameter values are misjudged by $\pm 10\%$. Between two tongue-shaped red shade regions there are areas with drop of the probability up to 0.5. From the practical point of view, only the left red-shaded region provides stability of the operation of the device in the desired manner. All other areas on the plots suggest that the stability of the cross-well motion is minor and it may easily jump to another type of stable motion.

Our analysis revealed variations in how the four energy harvesters responded to parameter mismatch. Electromagnetic harvesters (S1 and S2) exhibited similar behavior, with S2 (being more complex) demonstrating greater basin stability across a wider range. However, S2 also had larger regions with a 50% chance of cross-well motion, indicating a higher probability of undesirable transitions despite overall basin stability. Both S1 and S2 showed minimal impact from $\pm 2.5\%$ parameter mismatch, but $\pm 10\%$ variations significantly reduced the probability of reaching cross-well motion (up to 50% decrease). Piezoelectric harvesters (S3 and S4) displayed superior resistance to parameter mismatch, maintaining stability in regions with dominant basin attraction. This is evident in Figures 5, 6, and the darker blue shades in Figure 7 (panels c & d), indicating maximum absolute stability changes of 23% (S3) and 30% (S4) even with $\pm 10\%$ mismatch. Maximum absolute differences in basin stability for different systems are gathered in the table below:

Degree of parameter mismatch	Maximum absolute basin stability change			
	S1	S2	S3	S4
$\pm 2.5\%$	0.75	0.23	0.16	0.22
$\pm 5\%$	0.74	0.30	0.27	0.23
$\pm 10\%$	0.75	0.54	0.23	0.30

4 Conclusions

This study investigated the influence of parameter mismatch on the stability of cross-well motion in four energy harvesters using a basin stability metric. We showed how different percentages of mismatch alter the system dynamics. Our results demonstrate that piezoelectric harvesters exhibited greater resilience to parameter variations compared to electromagnetic designs, which should be further investigated. Safe operating ranges, in considered parameter space, identified through basin stability analysis offer valuable insights for engineers and scientists to ensure stable cross-well motion despite potential parameter uncertainties. These findings highlight the influence of parameter mismatch on the design and operation of energy harvesters.

Acknowledgment

This paper has been completed while the first author was the Doctoral Candidate in the Interdisciplinary Doctoral School at the Lodz University of Technology, Poland.

This work is funded by the National Science Center Poland based on the decision number 2018/31/D/ST8/02439.

References

- [1] Mahmoud M. Magdy, Nader A. Mansour, Ahmed M.R. Fath El-Bab, and Samy F.M. As-sal. Human motion spectrum-based 2-dof energy harvesting device: Design methodology and experimental validation. *Procedia Engineering*, 87:1218–1221, 2014. EUROSENSORS 2014, the 28th European Conference on Solid-State Transducers.
- [2] Ihor Sobianin, Sotiria Psoma, and A. Tournlidakis. Recent advances in energy harvesting from the human body for biomedical applications. *Energies*, 15:7959, 10 2022.
- [3] Bingqiang Shan, Tengtian Ai, and Kai Wang. Triboelectric nanogenerator for ocean energy harvesting: A review of technological advances and future perspectives. *International Journal of Electrochemical Science*, 19(8):100694, 2024.
- [4] Mengzhou Liu, Yuan Zhang, Hailing Fu, Yong Qin, Ao Ding, and Eric M. Yeatman. A seesaw-inspired bistable energy harvester with adjustable potential wells for self-powered internet of train monitoring. *Applied Energy*, 337:120908, 2023.

- [5] Petr Sosna, Ondřej Rubeš, and Zdenek Hadaš. Verification and analysis of advanced tuneable nonlinear vibration energy harvester. *Mechanical Systems and Signal Processing*, 189:110096, 2023.
- [6] Xuefeng Li, Daniil Yurchenko, Renfu Li, Xingxing Feng, Bo Yan, and Kai Yang. Performance and dynamics of a novel bistable vibration energy harvester with appended nonlinear elastic boundary. *Mechanical Systems and Signal Processing*, 185:109787, 2023.
- [7] Jianwei Zhang, Mengyao Wu, Haofeng Wu, and Shuaimin Ding. An asymmetric bistable vibro-impact deg for enhanced ultra-low-frequency vibration energy harvesting. *International Journal of Mechanical Sciences*, 255:108481, 2023.
- [8] Wei Wang, Jianhui Wang, Shuangyan Liu, and Ronghan Wei. Nonlinear dynamics and performance evaluation of an asymmetric bistable energy harvester with unilateral piecewise nonlinearity. *Nonlinear Dynamics*, 112(10):8043–8069, April 2024.
- [9] Kunming Chen, Xiao Zhang, Xiaoyi Xiang, Hui Shen, Qian Yang, Junlei Wang, and Grzegorz Litak. High performance piezoelectric energy harvester with dual-coupling beams and bistable configurations. *Journal of Sound and Vibration*, 561:117822, 2023.
- [10] Shun Chen and Liya Zhao. A quasi-zero stiffness two degree-of-freedom nonlinear galloping oscillator for ultra-low wind speed aeroelastic energy harvesting. *Applied Energy*, 331:120423, 2023.
- [11] Qingzhao Li, Ling Bu, Shiyu Lu, Bowen Yao, Qianming Huang, and Xiaohong Wang. Practical asymmetry and its effects on power and bandwidth performance in bi-stable vibration energy harvesters. *Mechanical Systems and Signal Processing*, 206:110939, 2024.
- [12] Lin Chen, Xin Liao, Guofeng Xia, Beibei Sun, and Yang Zhou. Variable-potential bistable nonlinear energy sink for enhanced vibration suppression and energy harvesting. *International Journal of Mechanical Sciences*, 242:107997, 2023.
- [13] Wei Tang, Zhenwei Chen, Ye Wang, and Bo Wang. High-energy response activation for bistable energy harvester with variable damping control. *Sensors and Actuators A: Physical*, 350:114110, 2023.
- [14] Yucheng Yan, Qichang Zhang, Jianxin Han, Wei Wang, Tian Wang, Xinyu Cao, and Shuying Hao. Design and investigation of a quad-stable piezoelectric vibration energy harvester by using geometric nonlinearity of springs. *Journal of Sound and Vibration*, 547:117484, 2023.

- [15] Maciej Leszczyński, Przemysław Perlikowski, Tomasz Burzyński, Tomasz M. Kowalski, and Piotr Brzeski. Review of sample-based methods used in an analysis of multi-stable dynamical systems. *Chaos: An Interdisciplinary Journal of Nonlinear Science*, 32(8):082101, 08 2022.
- [16] P. Brzeski, J. Wojewoda, T. Kapitaniak, J. Kurths, and P. Perlikowski. Sample-based approach can outperform the classical dynamical analysis - experimental confirmation of the basin stability method. *Scientific Reports*, 7(1):6121, 2017.
- [17] P. Brzeski, M. Lazarek, T. Kapitaniak, J. Kurths, and P. Perlikowski. Basin stability approach for quantifying responses of multistable systems with parameters mismatch. *Meccanica*, 51(11):2713–2726, November 2016. Acknowledgement This work is funded by the National Science Center Poland based on the decision number DEC-2015/16/T/ST8/00516. PB is supported by the Foundation for Polish Science (FNP).
- [18] Peter J. Menck, Jobst Heitzig, Norbert Marwan, and Jürgen Kurths. How basin stability complements the linear-stability paradigm. *Nature Physics*, 9(2):89–92, 2013.
- [19] Dirk Spreemann, Daniel Hoffmann, Bernd Folkmer, and Yiannos Manoli. Numerical optimization approach for resonant electromagnetic vibration transducer designed for random vibration. *Journal of Micromechanics and Microengineering*, 18(10):104001, sep 2008.
- [20] Abu Riduan Md. Foisal, Chinsuk Hong, and Gwiyoung Sang Chung. Multi-frequency electromagnetic energy harvester using a magnetic spring cantilever. *Sensors and Actuators A: Physical*, 182:106–113, 2012.
- [21] Luã G. Costa and Marcelo A. Savi. Nonlinear dynamics of a compact and multistable mechanical energy harvester. *International Journal of Mechanical Sciences*, 262:108731, 2024.
- [22] José G. Etse, Bibiana M. Luccioni, Martín A. Pucheta, and Mario Alberto Storti. Lagrangians for electromechanical systems. 2018.
- [23] Krzysztof Kecik, Piotr Brzeski, and Przemysław Perlikowski. Non-linear dynamics and optimization of a harvester-absorber system. *International Journal of Structural Stability and Dynamics*, 17(05):1740001, 2017.